

Lawrence Berkeley National Laboratory

LBL Publications

Title

The magnetic order in multiferroic DyMnO₃

Permalink

<https://escholarship.org/uc/item/1kp091wq>

Authors

Lee, Jenn-Min
Huang, Shih-Wen
Jeng, Horng-Tay
[et al.](#)

Publication Date

2021

DOI

10.1016/j.elspec.2020.147013

Peer reviewed

The magnetic order in multiferroic DyMnO₃

Jenn-Min Lee^{a,b}, Shih-Wen Huang^{a,c,d,**}, Horng-Tay Jeng^e, Yu-Cheng Shao^{f,c}, L. Andrew Wray^g, Jin Ming Chen^b, Ruimin Qiao^c, Wanli Yang^c, Jiunn-Yuan Lin^h, Robert W. Schoenlein^d, Yi-De Chuang^{c,**}

^aMAX IV Laboratory, Lund University, P. O. Box 118, 221 00 Lund, Sweden

^bNational Synchrotron Radiation Research Center, Hsinchu 30076, Taiwan

^cAdvanced Light Source, Lawrence Berkeley National Laboratory, Berkeley, CA 94720, USA

^dMaterials Sciences Division, Lawrence Berkeley National Laboratory, Berkeley, CA 94720, USA

^eDepartment of Physics, National Tsing Hua University, Hsinchu 30013, Taiwan

^fDepartment of Physics, Tamkang University, Taipei 25137, Taiwan

^gDepartment of Physics, New York University, New York, NY 10003, USA

^hInstitute of Physics, National Chiao Tung University, Hsinchu 300, Taiwan

Abstract

With flexibility in tuning their electric and magnetic properties, multiferroics can be used in information exchange and storage in ways that are very different from the present electronic materials. Here we use resonant soft x-ray scattering spectroscopy to study the *F*-type $(0, \tau, 0)$ and *C*-type $(0, 1-2\tau, 0)$ diffraction peaks from sinusoidal antiferromagnetic spin order in multiferroic DyMnO₃. By comparing the temperature dependence of ordering wave vectors τ , peak intensities I , and correlation lengths λ measured at Mn L_2 -, O K -, and Dy M_5 -edges, we show that the nearly perfect locking between the ordering wave vectors from Dy $4f$ states and Mn $3d$ orbitals manifesting the second harmonic diffraction peak implies the notable orbital involvement in the coupling between Mn and Dy spins. Our DFT calculations further suggest that the lattice response to different antiferromagnetic ground states (A-type versus E-type) is much weaker in TbMnO₃, in agreement with previous claim that the symmetric exchange interaction can be an important factor for understanding the ferroelectricity in

*Corresponding author

**Corresponding author

Email addresses: shih-wen.huang@maxiv.lu.se (Shih-Wen Huang), ychuang@lbl.gov (Yi-De Chuang)

DyMnO₃ than in TbMnO₃.

Keywords: Multiferroic, resonant x-ray scattering

1. Introduction

In response to the growing demands on energy to sustain the human civilization, modern electronic devices are becoming more powerful, compact, and energy efficient. However, this evolutionary trend for electronic devices will soon reach the bottleneck around nm critical dimension where pending issues such as the proper choice of materials to prevent dielectric breakdown, the precise control of dopants inside semiconductors, the methodology of EUV lithography, the advanced metrologies to resolve finer spatial features, ... etc. remain the daunting technology challenges. On the other hand, current electronic devices only use the charge degree of freedom of electrons and proposals to tap into other degrees such as spin and/or orbital can be attractive because they offer additional dimensions to manipulate the digital information. But to realize these novel devices, one needs materials with two or more functionalities emerging from the interactions between multiple electronic degrees of freedom.

Materials that exhibit two or more ferroic orders, such as ferroelasticity, ferroelectricity, and ferromagnetism (or antiferromagnetism), are known as multiferroics. Although multiferroics can be attractive candidates for next generation electronic devices that will employ all electronic degrees of freedom, it is not easy to find them.[1, 2, 3, 4, 5] Taking the coexistence of ferroelectricity and ferromagnetism as an example, these two ferroic orders are quite different from the symmetry point of view: ferroelectricity is associated with broken inversion symmetry while ferromagnetism is associated with broken time-reversal symmetry. From the electronic point of view, partially filled d orbitals in transition metal elements are important for ferromagnetism, but ferroelectricity favors ions with empty d orbitals.

Recently, the so-called type-II multiferroic manganites $RMnO_3$ and RMn_2O_5 (R : rare earth elements) whose ferroelectricity is induced by complex magnetic

orders have been demonstrated to exhibit strong magnetoelectric effect.[6, 7, 8, 9, 10, 11, 11, 12, 13, 14] With respect to temperature, they often go through a series of magnetic transitions with distinct magnetic orders and electric properties, as illustrated in Figure 1(a) for DyMnO₃. When subjected to magnetic field or electric field, their responses also vary significantly.[15, 16, 17, 18] These multiferroic manganites offer us the opportunity to control one order through perturbations that influence the other electronic degree of freedom.[1, 19, 20, 21, 22, 23] This aspect, in particular using electric field (charge degree of freedom) and magnetic field (spin degree of freedom) to control ferromagnetism and ferroelectricity, respectively, makes them extremely useful for electronic technologies because the flexibility in changing the charge and spin states of electrons provides other means to exchange and store digital information.

Several mechanisms, such as anti-symmetric inverse Dzyaloshinskii-Moriya (DM) interaction (spin current),[24, 25, 26] symmetric Heisenberg exchange interaction (exchange striction),[27, 28, 29, 30] spin-dependent Mn-ligand *p-d* hybridization,[31] and other degrees of freedom such as orbital and lattice,[32, 33, 34, 35, 36, 37, 38, 39] have been proposed to explain the ferroelectricity in these manganites.[21, 22] Previously, we used resonant soft x-ray scattering (RSXS) spectroscopy to study the first harmonic *F*-type (0, τ , 0) diffraction peak produced by the sinusoidal antiferromagnetic spin order in multiferroic DyMnO₃ and TbMnO₃ to show that the aforementioned mechanisms can play different roles in the ferroelectric transitions. In particular, we pointed out that besides the structural based mechanisms, the electronic correlation is an important ingredient to understand the ferroelectricity in DyMnO₃. [40]

Here, we look at the second harmonic *C*-type (0, 1-2 τ , 0) peak of DyMnO₃ measured at Mn *L*₂-edge. Compared with τ^{Mn} determined from first harmonic peak, τ^{Mn} from second harmonic peak tracks τ^{Dy} even more closely. Furthermore, the anomalous temperature dependence around the ferroelectric transition is also seen in the correlation length λ of second harmonic peak, corroborating with previous findings in first harmonic peak. By performing similar DFT calculations, we notice that the variant in magnetic ground states has weaker

effect on the structure of TbMnO₃ compared to DyMnO₃. The calculations are
 60 consistent with the proposal that the proximity to E-type antiferromagnetism
 is an important factor in understanding the ferroelectricity in DyMnO₃ as well.

2. Results and Discussions

Selected q -scans at O K - and Mn L_2 -edges are shown in Figures 1(b) and
 (c, d), respectively. Due to multiple absorption edges used in this study, we
 65 adopt the following convention to simplify the discussion: O, Mn, and Dy in the
 superscript of τ , I , and λ indicate the results from measurements at O K -, Mn
 L_2 -, and Dy M_5 -edges. 1 and 2 indicate the results for $(0, \tau, 0)$ (first harmonic)
 and $(0, 1-2\tau, 0)$ (second harmonic) diffraction peaks.

Below the Neel temperature $T_N \sim 39$ K, Mn spins form a collinear sinu-
 70 soidal antiferromagnetic order along the crystalline \hat{b} -axis. This magnetic order
 produces the first harmonic F -type $(0, \tau^{\text{Mn}}, 0)$ (Figure 1(c), $h\nu=645.4$ eV) and
 second harmonic C -type $(0, 1-2\tau^{\text{Mn}}, 0)$ (Figure 1(d), $h\nu=645.8$ eV) diffraction
 peaks that can be accessed using soft x-rays. **The first harmonic directly comes**
from magnetic order from Mn sites while **\mp** the second harmonic peak comes
 75 from the quadratic term in the magnetoelastic coupling between lattice and
 spin degrees of freedom, and **is** **are all** influenced by Mn $3d$ orbitals. When the
 sample temperature is increased, like $(0, \tau^{\text{O}}, 0)$, both first and second harmonic
 peaks become weaker, consistent with the literatures.[12, 41, 42, 43, 44, 45, 46,
 47, 48, 49, 50, 51] However, close examination shows that they have different
 80 intensity and width behaviors: the $(0, 1-2\tau^{\text{Mn}}, 0)$ peak exhibits more dras-
 tic decrease in intensity above 20 K and has a broader width (or equivalently,
 shorter correlation length) throughout the temperature range. In Figure 1(e),
 we show $h\nu$ -scans at $(h, k, l)=(0, \tau^{\text{Mn}}, 0)$ (top) and $(0, 1-2\tau^{\text{Mn}}, 0)$ (bottom)
 at $\tau^{\text{Mn}}=0.385$ and 13 K. From the distinct incident photon energy dependence
 85 (the resonance profile), it is clear that their contrasting behaviors are related
 to different electronic states involved in producing these diffraction peaks. To
 quantify the differences, the Lorentzian fitting was performed on q -scans and

results are summarized in Figures 2(a)-2(h).

We overlay τ^{Mn} s from $(0, \tau, 0)$ (blue open circles, $\tau^{\text{Mn},1}$) and $(0, 1-2\tau, 0)$ (green filled circles, $\tau^{\text{Mn},2}$) diffraction peaks with τ^{Dy} from $(0, \tau, 0)$ peak (red filled diamonds) in Figures 2(a) and 2(b), respectively. The difference $\Delta\tau = \tau^{\text{Dy}} - \tau^{\text{Mn}}$ is shown in the top panels. From the temperature dependence of $\Delta\tau$, one can see that $\tau^{\text{Mn},2}$ tracks τ^{Dy} more closely than $\tau^{\text{Mn},1}$, with the magnitude of $\Delta\tau$ less than half of that of $\tau^{\text{Mn},1}$. The agreement can also be seen in the intensity and correlation length behaviors. The intensities $I^{\text{Mn},1}$ (Figure 2(c)), $I^{\text{Mn},2}$ (Figure 2(e)), and I^{Dy} (Figure 2(g)) all exhibit monotonic decrease with increasing sample temperature. A kink that marks the onset of linear temperature dependence at high temperature (the dashed color lines are guides for eyes) is observed in all curves around $20 \sim 25$ K, just above the ferroelectric transition temperature $T_{\text{FE}}=19$ K (the ferroelectric phase is shown as blue shaded region). However, the magnitude of this kink is much larger in $I^{\text{Mn},2}$ and I^{Dy} . For $\lambda^{\text{Mn},1}$ (Figure 2(d)), $\lambda^{\text{Mn},2}$ (Figure 2(f)), and λ^{Dy} (Figure 2(h)), they all show larger values above the ferroelectric transition, but the anomalous reduction seen in λ^{Dy} is also observed in $\lambda^{\text{Mn},2}$. Previously, we argued that this anomaly is not due to fitting artifacts and can be attributed to the symmetric exchange coupling $H_{df} = g_{\mu_B} \sum_i \vec{s}_i \cdot \vec{H}_{\text{in}}$ between Mn and Dy spins.[40] Observing similar behavior in $\lambda^{\text{Mn},2}$ that has comparable magnitude substantiates the authenticity of this anomaly. The similarity between the $(0, 1-2\tau, 0)$ peak measured at Mn L_2 -edge and the $(0, \tau, 0)$ peak measured at Dy M_5 -edge implies that the strong coupling between Mn and Dy spins involve Mn $3d$ orbitals as well.

Although DyMnO_3 and TbMnO_3 are the prototypical multiferroics that have been extensively studied over the past years, the former one has more than three times the electric polarization ($P_s \sim 0.2\mu\text{C}/\text{cm}^2$) than the latter one and is more attractive from the perspective of electronic technology applications. One plausible reason for the enhanced electric polarization is the coherence spin configuration of Mn and Dy below T_N . When going from La to Ho, the size of rare earth ion decreases; consequently, the lattice distortion is enhanced through tilting and deformation of MnO_6 octahedral. With enhanced lattice distortion,

the strength of spin interactions are modified such that the magnetic ground
 120 state evolves from A-type (LaMnO₃) to collinear sinusoidal (Tb/DyMnO₃) to E-
 type antiferromagnetism (HoMnO₃). [7, 9] In addition, the tendency for orbital
 mixing and orbital ordering becomes stronger. [52, 53, 54]

Previously, we carried out DFT calculations with A-type and E-type antifer-
 romagnetism that do not naturally occur in DyMnO₃ and investigated the effect
 125 of magnetic ground states on Mn 3*d* orbitals. We showed that with E-type an-
 tiferromagnetism, the lattice structure is further distorted after relaxation **with
 four inequivalent in-plane Mn-O bands**, that leads to more delocalized **Mn 3*d*
 p** orbitals. Based on that result, we argued that the proximity to E-type anti-
 ferromagnetism may enhance **Mn and neighboring oxygen** orbital hybridizations
 130 in DyMnO₃. Here, we perform similar DFT calculations on TbMnO₃ and com-
 pare results from DyMnO₃. The calculated spin polarized partial density of
 states (pDOS) of Mn in DyMnO₃ (left panels) and TbMnO₃ (right panels) are
 summarized in Figure 3. In this figure, the A-type (top panels) and E-type (bot-
 tom panels) antiferromagnetism are employed with proper lattice relaxation to
 135 attain the ground states.

The DFT calculations reproduce the insulating ground states for both ma-
 terials with similar Mn 3*d* pDOS (up and down arrows in the figure denote the
 majority and minority spins, respectively). Upon changing the magnetic ground
 state from A-type to E-type antiferromagnetism, the majority $3d_{3x^2-r^2/3y^2-r^2}$
 140 orbitals (blue) in valence band are pushed up in energy, resulting in more spec-
 tral weight **near the Fermi energy near the top of valence band**. In addition,
 the majority $3d_{x^2-z^2/y^2-z^2}$ orbitals in conduction band become narrower. In
 fact, band-narrowing is a generic trend for Mn 3*d* orbitals with E-type antifer-
 romagnetism for DyMnO₃ and TbMnO₃, and this effect pushes the rare earth
 145 *d* bands to even higher energy [data not shown in the figure].

Noticing that the band profiles can change significantly with respect to the
 magnetic ground states, we now look at their variants in the spatial distribu-
 tion. The pDOS is integrated over [-0.74 eV, 0 eV] energy window to produce
 the iso-charge surface, which are shown in Figure 4. In this figure, we only show

150 the results with relaxed E-type antiferromagnetism. The Mn-O bond lengths
 (Mn-O(1): out-of-plane bonds; Mn-O(2): in-plane bonds) for DyMnO₃ (DMO)
 and TbMnO₃ (TMO) using different magnetic ground states with and without
 lattice relaxation are summarized in Table I. Like in previous study for ~~both~~
 DyMnO₃ ~~and,~~ [40] ~~the lattice structure for TbMnO₃ also, the lattice structure~~
 155 becomes more asymmetrically distorted in-plane when going from A-type to
 E-type antiferromagnetism, reflecting the loss of local mirror symmetry [~~the~~
~~difference between two inequivalent Mn-O(2) bond pairs is increased from A-~~
~~type to E-type antiferromagnetism].~~ In the meantime, the Mn 3d orbitals be-
 come more delocalized as expected. What is intriguing from DFT calculations
 160 is that for TbMnO₃, the effect of lattice relaxation with respect to different
 magnetic ground states is much smaller compared to DyMnO₃ (see boldface
 numbers in Table I ; ~~numbers in () are the differences in the bond length with-~~
~~out and with lattice relaxation).~~ This implies that contrary to DyMnO₃, the
 exact choice of magnetic ground state (or proximity to A-type or E-type antifer-
 165 romagnetism) plays a minor role in affecting the energetics of TbMnO₃. ~~From~~
~~previous study, [40] we showed that the wave vector of F-type (0, τ , 0) diffraction~~
~~peak for DyMnO₃ and TbMnO₃ displays contrasting temperature dependence~~
~~where upon lowering the temperature, the former one increases continuously~~
~~from 0.365 to 0.385 while the latter one reduces from 0.30 down to 0.285 at~~
 170 ~~17 K. Since DFT calculation shows that the choice of exact magnetic ground~~
~~state has a weaker effect on the structure of TbMnO₃ relative to DyMnO₃, it is~~
~~reasonable to expect that the wave vector of TbMnO₃ magnetic order can de-~~
~~viate from the E-type antiferromagnetism (wave vector around 0.354) without~~
~~the significant energetic penalty from the spin-lattice interaction. On the other~~
 175 ~~hand, the tracking of the wave vector of C-type (0, 1-2 τ , 0) (from magnetoe-~~
~~lastic coupling) of Mn spin and F-type (0, τ , 0) of Dy spin (Fig. 2(b)) reflects~~
~~the important role of structural influence that keeps these wave vectors around~~
~~that of the E-type antiferromagnetism. This may explain why the spin ordering~~
~~vectors for DyMnO₃ and TbMnO₃ evolve differently at low temperature where~~
 180 ~~the later one deviates further from the E-type antiferromagnetic wave vector.~~

3. Summary

We have used RSXS spectroscopy to study the second harmonic C -type $(0, 1-2\tau, 0)$ diffraction peak in multiferroic DyMnO_3 . We show that the wave vector of sinusoidal antiferromagnetic spin order determined from this second harmonic peak at Mn L_2 -edge ($\tau^{\text{Mn},2}$) tracks that of the first harmonic peak at Dy M_5 -edge (τ^{Dy}) much more closely. Furthermore, the anomalous reduction in the correlation length just above the ferroelectric transition seen previously in λ^{Dy} is also observed in $\lambda^{\text{Mn},2}$. The similarity between these two diffraction peaks implies that the strong coupling between Mn and Dy spins has noticeable Mn $3d$ orbital involvement. We also carry out DFT calculations to look at the effect of different magnetic ground states on Mn $3d$ orbitals. Contrary to DyMnO_3 , we notice that the lattice response to different antiferromagnetic ground states with and without lattice relaxation is much smaller in TbMnO_3 . The weak response is in agreement with the notion that the proximity to E-type antiferromagnetism plays a more important role in DyMnO_3 than TbMnO_3 .

4. Materials and Methods

Single crystal DyMnO_3 was grown by flux method and the details of crystal growth can be found elsewhere.[55, 56] The crystal was checked by conventional four-circle diffractometry to confirm the orthorhombically distorted perovskite structure with $Pbnm$ space group ($a = 5.28 \text{ \AA}$, $b = 5.85 \text{ \AA}$, $c = 7.38 \text{ \AA}$). Since the natural growth produces the $[1, 1, 0]$ surface, the $[0, 1, 0]$ and $[0, 0, 1]$ surfaces were aligned in the horizontal scattering plane by mounting the sample on a 45° wedge. RSXS measurements were carried out at Beamline 8.0.1 at the Advanced Light Source (ALS), Lawrence Berkeley National Laboratory (LBNL), using the RSXS endstation.[57] During measurements, the incident photon polarization was kept in the horizontal scattering plane (π -scattering geometry). The beamline energy resolution was better than 0.3 eV, 0.25 eV, and 0.2 eV at O K - (523.75 eV), Mn L_2 - (645.4 eV/645.8 eV), and Dy M_5 -edges (1290 eV),

respectively. The beam spot on the sample was around $40 \mu\text{m}$ (v) by $500 \mu\text{m}$
210 (h). All temperature dependence spectra were recorded in the warming process.

A photodiode with front Al window to block out ambient light and photoelectrons was used to record the scattered x-rays from sample. The angular resolution of this photodiode was $\sim 0.5^\circ$, better than the half-width half-maximum (HWHM) of diffraction peaks. Two types of spectra were recorded
215 and presented in this paper: $h\nu$ - and q -scans. For q -scans, the incident photon energy was fixed while sample (θ) and detector angles were varied so that photon momentum transfer was projected along the crystalline \hat{b} -axis. In the current study, the sample and detector angles followed θ - 2θ relationship. For $h\nu$ -scans, the incident photon energy, sample, and detector angles were changed
220 simultaneously to keep the photon momentum transfer at a specific \vec{q} -value. The q -scans were first normalized by incident photon flux determined from the photocurrent of an upstream Au mesh. The normalized spectra were then fitted with a Lorentzian function on top of a linear background to remove the contributions from fluorescence and specular reflection [these two contributions have
225 monotonic \vec{q} dependence]. The ordering wave vector τ was determined from the peak position. The intensity I shown in this paper is the peak area. The correlation length λ was calculated using the inverse of half-width half-maximum (HWHM) of Lorentzian peak.

The first principles calculations were carried using the accurate full-potential
230 augmented-wave method,[58, 59] as embodied in the Vienna *ab initio* simulation package (VASP). The exchange-correlation initiation was treated within the generalized gradient approximation (GGA+U). The calculations were performed over $7 \times 7 \times 5$ ($a \times b \times c$ unit cell) and $7 \times 3 \times 5$ ($a \times 2b \times c$ unit cell) Monkhorst-Pack k -point meshes in the irreducible Brillouin zone for A- and E-type antiferromagnetism, respectively. Lattice relaxation, which gives
235 lower energy, was also included in the calculations. The on-site Coulomb energy $U = 5.0$ eV and exchange energy $J = 0.87$ eV were used for Mn $3d$ electrons.[56]

Acknowledgement

The Advanced Light Source is supported by the Director, Office of Science,
240 Office of Basic Energy Sciences, of the U.S. Department of Energy under Con-
tract No. DE-AC02-05CH11231. Work by J. Y. L. was financially supported by
the MOST of Taiwan, under the Grant 103-2112-M-009-007-MY3 and the Cen-
ter for Emergent Functional Matter Science of National Chiao Tung University
from The Featured Areas Research Center Program within the framework of
245 the Higher Education Sprout Project by the Ministry of Education (MOE) in
Taiwan.

References

- [1] N. A. Spaldin, M. Fiebig, The renaissance of magnetoelectric multiferroics,
Science 309 (5733) (2005) 391–392. [doi:10.1126/science.1113357](https://doi.org/10.1126/science.1113357).
- 250 [2] C. RayanáSerrao, et al., New routes to multiferroics, Journal of Materials
Chemistry 17 (47) (2007) 4931–4938. [doi:10.1039/B709126E](https://doi.org/10.1039/B709126E).
- [3] W. Eerenstein, N. Mathur, J. F. Scott, Multiferroic and magnetoelectric
materials, nature 442 (7104) (2006) 759–765. [doi:10.1038/nature05023](https://doi.org/10.1038/nature05023).
- [4] J. Scott, Applications of modern ferroelectrics, science 315 (5814) (2007)
255 954–959. [doi:10.1126/science.1129564](https://doi.org/10.1126/science.1129564).
- [5] R. Ramesh, Emerging routes to multiferroics, Nature 461 (7268) (2009)
1218–1219. [doi:10.1038/4611218a](https://doi.org/10.1038/4611218a).
- [6] T. Kimura, T. Goto, H. Shintani, K. Ishizaka, T.-h. Arima, Y. Tokura,
Magnetic control of ferroelectric polarization, nature 426 (6962) (2003) 55–
260 58. [doi:10.1038/nature02018](https://doi.org/10.1038/nature02018).
- [7] T. Kimura, S. Ishihara, H. Shintani, T. Arima, K. T. Takahashi,
K. Ishizaka, Y. Tokura, Distorted perovskite with e_g^1 configuration as a
frustrated spin system, Phys. Rev. B 68 (2003) 060403. [doi:10.1103/
PhysRevB.68.060403](https://doi.org/10.1103/PhysRevB.68.060403).

- 265 [8] N. Hur, S. Park, P. Sharma, J. Ahn, S. Guha, S.-W. Cheong, Electric polarization reversal and memory in a multiferroic material induced by magnetic fields, *Nature* 429 (6990) (2004) 392–395. [doi:10.1038/nature02572](https://doi.org/10.1038/nature02572).
- [9] T. Goto, T. Kimura, G. Lawes, A. P. Ramirez, Y. Tokura, Ferroelectricity and giant magnetocapacitance in perovskite rare-earth manganites, *Phys. Rev. Lett.* 92 (2004) 257201. [doi:10.1103/PhysRevLett.92.257201](https://doi.org/10.1103/PhysRevLett.92.257201).
270
- [10] T. Kimura, G. Lawes, T. Goto, Y. Tokura, A. P. Ramirez, Magnetolectric phase diagrams of orthorhombic $r\text{mno}_3$ ($r = \text{Gd}, \text{tb}, \text{and dy}$), *Phys. Rev. B* 71 (2005) 224425. [doi:10.1103/PhysRevB.71.224425](https://doi.org/10.1103/PhysRevB.71.224425).
- [11] M. Kenzelmann, A. B. Harris, S. Jonas, C. Broholm, J. Schefer, S. B. Kim, C. L. Zhang, S.-W. Cheong, O. P. Vajk, J. W. Lynn, Magnetic inversion symmetry breaking and ferroelectricity in tbmno_3 , *Phys. Rev. Lett.* 95 (2005) 087206. [doi:10.1103/PhysRevLett.95.087206](https://doi.org/10.1103/PhysRevLett.95.087206).
275
- [12] R. Feyerherm, E. Dudzik, N. Aliouane, D. N. Argyriou, Commensurate dy magnetic ordering associated with incommensurate lattice distortion in multiferroic dymno_3 , *Phys. Rev. B* 73 (2006) 180401. [doi:10.1103/PhysRevB.73.180401](https://doi.org/10.1103/PhysRevB.73.180401).
280
- [13] T. Arima, T. Goto, Y. Yamasaki, S. Miyasaka, K. Ishii, M. Tsubota, T. Inami, Y. Murakami, Y. Tokura, Magnetic-field-induced transition in the lattice modulation of colossal magnetoelectric GdMnO_3 and TbMnO_3 compounds, *Phys. Rev. B* 72 (2005) 100102. [doi:10.1103/PhysRevB.72.100102](https://doi.org/10.1103/PhysRevB.72.100102).
285
- [14] T. Arima, A. Tokunaga, T. Goto, H. Kimura, Y. Noda, Y. Tokura, Collinear to spiral spin transformation without changing the modulation wavelength upon ferroelectric transition in $\text{tb}_{1-x}\text{dy}_x\text{mno}_3$, *Phys. Rev. Lett.* 96 (2006) 097202. [doi:10.1103/PhysRevLett.96.097202](https://doi.org/10.1103/PhysRevLett.96.097202).
290
- [15] N. Aliouane, D. N. Argyriou, J. Stremfper, I. Zegkinoglou, S. Landsgesell, M. v. Zimmermann, Field-induced linear magnetoelastic coupling in multi-

- ferroic tbmno_3 , Phys. Rev. B 73 (2006) 020102. [doi:10.1103/PhysRevB.73.020102](https://doi.org/10.1103/PhysRevB.73.020102).
- 295 [16] D. N. Argyriou, N. Aliouane, J. Stremper, I. Zegkinoglou, B. Bohnenbuck, K. Habicht, M. v. Zimmermann, Melting of incommensurate-ferroelectric phase with magnetic field in multiferroic tbmno_3 , Phys. Rev. B 75 (2007) 020101. [doi:10.1103/PhysRevB.75.020101](https://doi.org/10.1103/PhysRevB.75.020101).
- 300 [17] J. Stremper, B. Bohnenbuck, M. Mostovoy, N. Aliouane, D. N. Argyriou, F. Schrettle, J. Hemberger, A. Krimmel, M. v. Zimmermann, Absence of commensurate ordering at the polarization flop transition in multiferroic DyMnO_3 , Phys. Rev. B 75 (2007) 212402. [doi:10.1103/PhysRevB.75.212402](https://doi.org/10.1103/PhysRevB.75.212402).
- [18] R. Feyerherm, E. Dudzik, A. U. B. Wolter, S. Valencia, O. Prokhnenko, 305 A. Maljuk, S. Landsgesell, N. Aliouane, L. Bouchenoire, S. Brown, D. N. Argyriou, Magnetic-field induced effects on the electric polarization in rmno_3 ($r = \text{Dy, Gd}$), Phys. Rev. B 79 (2009) 134426. [doi:10.1103/PhysRevB.79.134426](https://doi.org/10.1103/PhysRevB.79.134426).
- [19] S.-W. Cheong, M. Mostovoy, Multiferroics: a magnetic twist for ferroelectricity, Nature materials 6 (1) (2007) 13–20. [doi:10.1038/nmat1804](https://doi.org/10.1038/nmat1804). 310
- [20] T. Kimura, Spiral magnets as magnetoelectrics, Annu. Rev. Mater. Res. 37 (2007) 387–413.
- [21] Y. Tokura, S. Seki, Multiferroics with spiral spin orders, Advanced materials 22 (14) (2010) 1554–1565. [doi:10.1002/adma.200901961](https://doi.org/10.1002/adma.200901961).
- 315 [22] Y. Tokura, S. Seki, N. Nagaosa, Multiferroics of spin origin, Reports on Progress in Physics 77 (7) (2014) 076501. [doi:10.1088/0034-4885/77/7/076501](https://doi.org/10.1088/0034-4885/77/7/076501).
- 320 [23] Y. Yamasaki, H. Sagayama, T. Goto, M. Matsuura, K. Hirota, T. Arima, Y. Tokura, Electric control of spin helicity in a magnetic ferroelectric, Phys. Rev. Lett. 98 (2007) 147204. [doi:10.1103/PhysRevLett.98.147204](https://doi.org/10.1103/PhysRevLett.98.147204).

- [24] H. Katsura, N. Nagaosa, A. V. Balatsky, Spin current and magnetoelectric effect in noncollinear magnets, *Phys. Rev. Lett.* 95 (2005) 057205. doi:
10.1103/PhysRevLett.95.057205.
- [25] M. Mostovoy, Ferroelectricity in spiral magnets, *Phys. Rev. Lett.* 96 (2006)
325 067601. doi:10.1103/PhysRevLett.96.067601.
- [26] I. A. Sergienko, E. Dagotto, Role of the dzyaloshinskii-moriya interaction
in multiferroic perovskites, *Phys. Rev. B* 73 (2006) 094434. doi:10.1103/
PhysRevB.73.094434.
- [27] M. Mochizuki, N. Furukawa, Microscopic model and phase diagrams of
330 the multiferroic perovskite manganites, *Phys. Rev. B* 80 (2009) 134416.
doi:10.1103/PhysRevB.80.134416.
- [28] M. Mochizuki, N. Furukawa, N. Nagaosa, Spin model of magnetostrictions
in multiferroic mn perovskites, *Phys. Rev. Lett.* 105 (2010) 037205. doi:
10.1103/PhysRevLett.105.037205.
- [29] M. Mochizuki, N. Furukawa, Theory of magnetic switching of ferroelec-
335 tricity in spiral magnets, *Phys. Rev. Lett.* 105 (2010) 187601. doi:
10.1103/PhysRevLett.105.187601.
- [30] S. Ishiwata, Y. Kaneko, Y. Tokunaga, Y. Taguchi, T.-h. Arima, Y. Tokura,
Perovskite manganites hosting versatile multiferroic phases with symmetric
340 and antisymmetric exchange strictions, *Phys. Rev. B* 81 (2010) 100411.
doi:10.1103/PhysRevB.81.100411.
- [31] C. Jia, S. Onoda, N. Nagaosa, J. H. Han, Microscopic theory of spin-
polarization coupling in multiferroic transition metal oxides, *Phys. Rev. B*
76 (2007) 144424. doi:10.1103/PhysRevB.76.144424.
- [32] D. V. Efremov, J. Van Den Brink, D. I. Khomskii, Bond-versus site-centred
345 ordering and possible ferroelectricity in manganites, *Nature materials* 3 (12)
(2004) 853–856. doi:10.1038/nmat1236.

- [33] S. Picozzi, K. Yamauchi, B. Sanyal, I. A. Sergienko, E. Dagotto, Dual nature of improper ferroelectricity in a magnetoelectric multiferroic, Phys. Rev. Lett. 99 (2007) 227201. doi:[10.1103/PhysRevLett.99.227201](https://doi.org/10.1103/PhysRevLett.99.227201).
350
- [34] J. J. Betouras, G. Giovannetti, J. van den Brink, Multiferroicity induced by dislocated spin-density waves, Phys. Rev. Lett. 98 (2007) 257602. doi:[10.1103/PhysRevLett.98.257602](https://doi.org/10.1103/PhysRevLett.98.257602).
- [35] S. Dong, R. Yu, S. Yunoki, J.-M. Liu, E. Dagotto, Origin of multiferroic spiral spin order in the $rmno_3$ perovskites, Phys. Rev. B 78 (2008) 155121. doi:[10.1103/PhysRevB.78.155121](https://doi.org/10.1103/PhysRevB.78.155121).
355
- [36] S. Dong, R. Yu, J.-M. Liu, E. Dagotto, Striped multiferroic phase in double-exchange model for quarter-doped manganites, Phys. Rev. Lett. 103 (2009) 107204. doi:[10.1103/PhysRevLett.103.107204](https://doi.org/10.1103/PhysRevLett.103.107204).
- [37] B. H. Kim, B. I. Min, Nearest and next-nearest superexchange interactions in orthorhombic perovskite manganites $rmno_3$ ($r =$ rare earth), Phys. Rev. B 80 (2009) 064416. doi:[10.1103/PhysRevB.80.064416](https://doi.org/10.1103/PhysRevB.80.064416).
360
- [38] J. L. Ribeiro, L. G. Vieira, Landau model for the phase diagrams of the orthorhombic rare-earth manganites $rmno_3$ ($r =$ Eu, gd, tb, dy, ho), Phys. Rev. B 82 (2010) 064410. doi:[10.1103/PhysRevB.82.064410](https://doi.org/10.1103/PhysRevB.82.064410).
365
- [39] M. Mochizuki, N. Furukawa, N. Nagaosa, Theory of spin-phonon coupling in multiferroic manganese perovskites $rmno_3$, Phys. Rev. B 84 (2011) 144409. doi:[10.1103/PhysRevB.84.144409](https://doi.org/10.1103/PhysRevB.84.144409).
- [40] S. W. Huang, J. M. Lee, H.-T. Jeng, Y. Shao, L. A. Wray, J. M. Chen, R. Qiao, W. L. Yang, Y. Cao, J.-Y. Lin, R. W. Schoenlein, Y.-D. Chuang, Prominent role of oxygen in the multiferroicity of $dymno_3$ and $tbmno_3$: A resonant soft x-ray scattering spectroscopy study, Phys. Rev. B 94 (2016) 035145. doi:[10.1103/PhysRevB.94.035145](https://doi.org/10.1103/PhysRevB.94.035145).
370
- [41] O. Prokhnenko, R. Feyerherm, E. Dudzik, S. Landsgesell, N. Aliouane, L. C. Chapon, D. N. Argyriou, Enhanced ferroelectric polarization by in-
375

- duced by spin order in multiferroic dymno_3 , Phys. Rev. Lett. 98 (2007) 057206. doi:10.1103/PhysRevLett.98.057206.
- [42] O. Prokhnenko, R. Feyerherm, M. Mostovoy, N. Aliouane, E. Dudzik, A. U. B. Wolter, A. Maljuk, D. N. Argyriou, Coupling of frustrated ising spins to the magnetic cycloid in multiferroic tbmno_3 , Phys. Rev. Lett. 99 (2007) 177206. doi:10.1103/PhysRevLett.99.177206.
- [43] J. Stremper, B. Bohnenbuck, I. Zegkinoglou, N. Aliouane, S. Landsgesell, M. v. Zimmermann, D. N. Argyriou, Magnetic-field-induced transitions in multiferroic tbmno_3 probed by resonant and nonresonant x-ray diffraction, Phys. Rev. B 78 (2008) 024429. doi:10.1103/PhysRevB.78.024429.
- [44] J. Voigt, J. Persson, J. W. Kim, G. Bihlmayer, T. Brückel, Strong coupling between the spin polarization of mn and tb in multiferroic TbMnO_3 determined by x-ray resonance exchange scattering, Phys. Rev. B 76 (2007) 104431. doi:10.1103/PhysRevB.76.104431.
- [45] N. Aliouane, O. Prokhnenko, R. Feyerherm, M. Mostovoy, J. Stremper, K. Habicht, K. C. Rule, E. Dudzik, A. U. B. Wolter, A. Maljuk, D. N. Argyriou, Magnetic order and ferroelectricity in RMnO_3 multiferroic manganites: coupling between r- and mn-spins, Journal of Physics: Condensed Matter 20 (43) (2008) 434215. doi:10.1088/0953-8984/20/43/434215. URL <https://doi.org/10.1088/0953-8984/20/43/434215>
- [46] R. A. Ewings, A. T. Boothroyd, D. F. McMorrow, D. Mannix, H. C. Walker, B. M. R. Wanklyn, X-ray resonant diffraction study of multiferroic Dymn_2O_5 , Phys. Rev. B 77 (2008) 104415. doi:10.1103/PhysRevB.77.104415.
- [47] T. Forrest, S. Bland, S. Wilkins, H. Walker, T. Beale, P. Hatton, D. Prabhakaran, A. Boothroyd, D. Mannix, F. Yakhou, et al., Ordering of localized electronic states in multiferroic tbmno_3 : a soft x-ray resonant scattering study, Journal of Physics: Condensed Matter 20 (42) (2008) 422205.

- [48] S. B. Wilkins, T. R. Forrest, T. A. W. Beale, S. R. Bland, H. C. Walker,
405 D. Mannix, F. Yakhou, D. Prabhakaran, A. T. Boothroyd, J. P. Hill, P. D.
Hatton, D. F. McMorrow, Nature of the magnetic order and origin of
induced ferroelectricity in tbmno_3 , Phys. Rev. Lett. 103 (2009) 207602.
[doi:10.1103/PhysRevLett.103.207602](https://doi.org/10.1103/PhysRevLett.103.207602).
- [49] T. A. W. Beale, S. B. Wilkins, R. D. Johnson, S. R. Bland, Y. Joly,
410 T. R. Forrest, D. F. McMorrow, F. Yakhou, D. Prabhakaran, A. T.
Boothroyd, P. D. Hatton, Antiferromagnetically spin polarized oxygen ob-
served in magnetoelectric tbmn_2o_5 , Phys. Rev. Lett. 105 (2010) 087203.
[doi:10.1103/PhysRevLett.105.087203](https://doi.org/10.1103/PhysRevLett.105.087203).
- [50] E. Schierle, V. Soltwisch, D. Schmitz, R. Feyerherm, A. Maljuk,
415 F. Yokaichiya, D. N. Argyriou, E. Weschke, Cycloidal order of $4f$ mo-
ments as a probe of chiral domains in dymno_3 , Phys. Rev. Lett. 105 (2010)
167207. [doi:10.1103/PhysRevLett.105.167207](https://doi.org/10.1103/PhysRevLett.105.167207).
- [51] U. Staub, Y. Bodenthin, M. García-Fernández, R. A. de Souza,
420 M. Garganourakis, E. I. Golovenchits, V. A. Sanina, S. G. Lushnikov, Mag-
netic order of multiferroic ermn_2o_5 studied by resonant soft x-ray bragg
diffraction, Phys. Rev. B 81 (2010) 144401. [doi:10.1103/PhysRevB.81.
144401](https://doi.org/10.1103/PhysRevB.81.144401).
- [52] G. Maris, V. Volotchaev, T. Palstra, Effect of ionic size on the orbital
ordering transition in $\text{rmno}_3 + \delta$, New Journal of Physics 6 (1) (2004) 153.
425 [doi:10.1088/1367-2630/6/1/153](https://doi.org/10.1088/1367-2630/6/1/153).
- [53] M. W. Kim, S. J. Moon, J. H. Jung, J. Yu, S. Parashar, P. Murugavel,
J. H. Lee, T. W. Noh, Effect of orbital rotation and mixing on the optical
properties of orthorhombic rmno_3 ($r = \text{La, pr, nd, gd, and tb}$), Phys. Rev.
Lett. 96 (2006) 247205. [doi:10.1103/PhysRevLett.96.247205](https://doi.org/10.1103/PhysRevLett.96.247205).
- 430 [54] F.-K. Chiang, M.-W. Chu, F. C. Chou, H. T. Jeng, H. S. Sheu, F. R.
Chen, C. H. Chen, Effect of jahn-teller distortion on magnetic ordering in

dy(fe,mn)o₃ perovskites, Phys. Rev. B 83 (2011) 245105. doi:10.1103/PhysRevB.83.245105.

435 [55] J. Chen, C. Chen, T. Chou, I. Jarrige, H. Ishii, K. Lu, Y. Cai, K. Liang, J. Lee, S. Huang, et al., Resonant x-ray emission spectroscopy of multi-ferroic tb mn o 3, Applied Physics Letters 91 (5) (2007) 054108. doi:10.1063/1.2762288.

440 [56] J. M. Chen, Z. Hu, H. T. Jeng, Y. Y. Chin, J. M. Lee, S. W. Huang, K. T. Lu, C. K. Chen, S. C. Haw, T. L. Chou, H.-J. Lin, C. C. Shen, R. S. Liu, A. Tanaka, L. H. Tjeng, C. T. Chen, Strong orbital polarization in orthorhombic dymno₃: A combined x-ray linear dichroism and ab initio electronic structure study, Phys. Rev. B 81 (2010) 201102. doi:10.1103/PhysRevB.81.201102.

445 [57] D. Doering, Y.-D. Chuang, N. Andresen, K. Chow, D. Contarato, C. Cummings, E. Domning, J. Joseph, J. Pepper, B. Smith, et al., Development of a compact fast ccd camera and resonant soft x-ray scattering endstation for time-resolved pump-probe experiments, Review of Scientific Instruments 82 (7) (2011) 073303. doi:10.1063/1.3609862.

450 [58] P. E. Blöchl, Projector augmented-wave method, Phys. Rev. B 50 (1994) 17953–17979. doi:10.1103/PhysRevB.50.17953.

[59] G. Kresse, D. Joubert, From ultrasoft pseudopotentials to the projector augmented-wave method, Phys. Rev. B 59 (1999) 1758–1775. doi:10.1103/PhysRevB.59.1758.

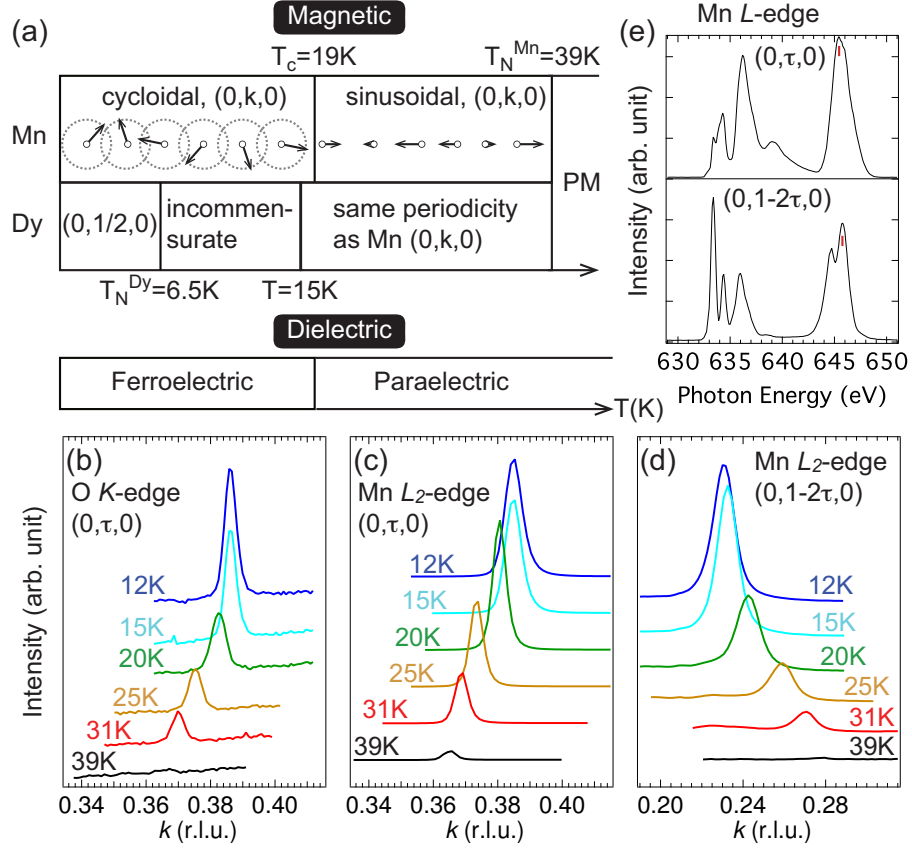


Figure 1: (color online) (a) Schematic plot showing the characteristic temperatures for magnetic orders for Mn and Dy spins and the electric properties. (b-d) Normalized q -scans at selected temperatures for (b) F -type $(0, \tau^O, 0)$ at O K -edge (523.75 eV), (c) F -type $(0, \tau^{Mn}, 0)$ at Mn L_2 -edge (645.4 eV) and (d) C -type $(0, 1-2\tau^{Mn}, 0)$ at Mn L_2 -edge (645.8 eV). Spectra are shifted vertically for clarity. (e) $h\nu$ -scans at $(0, \tau^{Mn}, 0)$ (top) and $(0, 1-2\tau^{Mn}, 0)$ (bottom) at 13 K, $\tau^{Mn} = 0.385$. The red vertical ticks show the photon energies used in recording the q -scans in panels (c) and (d).

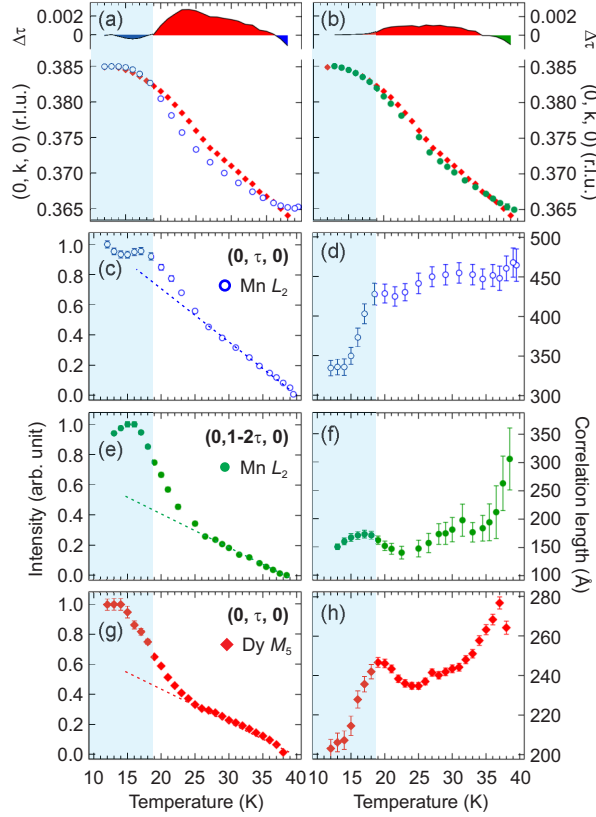


Figure 2: (color online) Lorentzian fitting results of q -scans showing the temperature dependence of (a, b) ordering wave vectors τ , (c, e, g) peak intensities I , and (d, f, h) correlation lengths λ . (a) Comparison of τ^{Dy} and $\tau^{\text{Mn},1}$. (b) Comparison of τ^{Dy} and $\tau^{\text{Mn},2}$. Top panels in (a) and (b) show the difference $\Delta\tau = \tau^{\text{Dy}} - \tau^{\text{Mn},1(2)}$. The $(\tau, I, \lambda)^{\text{Mn},1}$ (blue open circles), $(\tau, I, \lambda)^{\text{Mn},2}$ (green filled circles), and $(\tau, I, \lambda)^{\text{Dy}}$ (red filled diamonds) are determined from F -type $(0, \tau, 0)$, C -type $(0, 1-2\tau, 0)$, and F -type $(0, \tau, 0)$ diffraction peaks measured at Mn L_2 - (645.4 eV), Mn L_2 - (645.8 eV), and Dy M_5 -edges (1290 eV), respectively. The blue shaded area marks the ferroelectric phase. The dashed lines mark the linear temperature dependence at high temperature and are guides for eyes.

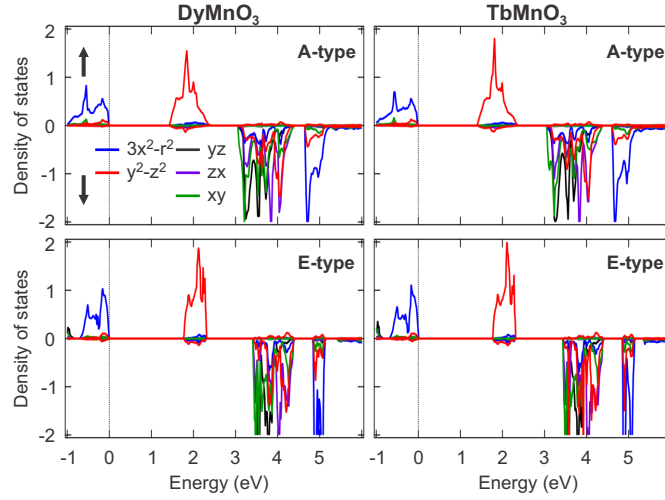


Figure 3: (color online) Spin polarized partial density of states (pDOS) of Mn in DyMnO_3 (left) and TbMnO_3 (right) with A-type (top) and E-type (bottom) antiferromagnetism. The up and down arrows indicate the majority and minority spins, respectively. The Mn s and p orbitals are located at much higher energies outside the display window.

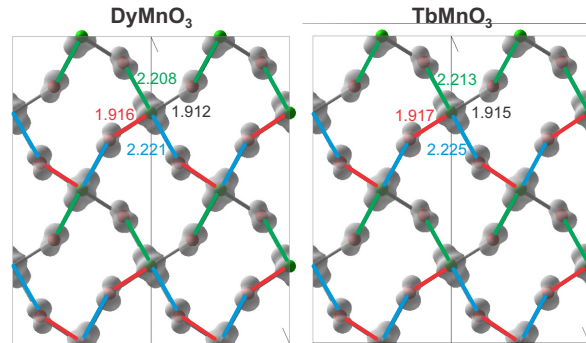


Figure 4: (color online) The in-plane iso-charge surface of DyMnO_3 (left) and TbMnO_3 (right) with relaxed E-type antiferromagnetism. The iso-charge surface is produced by integrating the DFT density of states in $[-0.74 \text{ eV}, 0 \text{ eV}]$ energy window.